Materials Science and Engineering B 271 (2021) 115260

Contents lists available at ScienceDirect

Materials Science & Engineering B

journal homepage: www.elsevier.com/locate/mseb

High-sensitivity and broadband PEDOT:PSS–silicon heterojunction photodetector

AliAkbar Noroozi [1], Amirhossein Mosaddegh [1], Yaser Abdi [*]

Nanophysics Research Laboratory, Department of Physics, University of Tehran, Tehran 14395-547, Iran

ARTICLE INFO

Keywords:
Hybrid organic-inorganic
Broadband
Photodetector

ABSTRACT

Recently we have shown that the poly(3,4-ethylenedioxythiophene): polystyrene sulfonate PEDOT:PSS/silicon hybrid heterojunctions possess great potential for light detection applications. Here we report fabrication of a broadband and high sensitive detector in both photo-current and photo-voltage mode. We propose PEDOT:PSS/silicon junction as a promising candidate for fabrication of high-sensitivity photodetector with responsivity as high as 90–230 mA/W in a broad range of incident light from UV to IR spectrum (from 350 to 950 nm), and responsivity up to 10^6 V/W in the self-powered photovoltage mode. The effect of organic layer conductivity on the responsivity of the detector is also studied here.

1. Introduction

Semiconductor heterojunctions are promising candidates for the fabrication of optoelectronic devices. As a major advantage, large bandgap semiconductors can be used as the top layer of the heterojunction where they serve as transparent window for the transmission of incoming light as well as charge collecting electrode. Despite the long history of all-inorganic counterparts, the hybrid organic–inorganic heterojunctions with the key property of low-temperature solution-based fabrication process have been considered just recently. As a stable highly-conductive organic material, poly(3,4-ethylenedioxythiophene) polystyrene sulfonate (PEDOT:PSS) has been used in a variety of hybrid organic–inorganic devices including solar cells [1–6], light-emitting diodes [7,8], transistors [9,10], and position-sensitive detectors [11,12]. In comparison with massive studies on PEDOT:PSS/Si solar cells [13–18], the optical signal detection capability of this hybrid heterojunction has received much less attention. Following a number of studies on the PEDOT:PSS/Si photo-detectors [19–21], we have recently uncovered the ultrahigh responsivity (10^6 V/W) of this heterojunction in the self-powered photovoltage mode, which indicates the huge potential of hybrid heterojunctions for optical signal detection [22]. Upon illumination to the heterojunction, the electric field at the depletion region separates the photo-generated electron-hole pairs so that the excess holes are transmitted to the p-type PEDOT:PSS and the excess electrons are pushed toward the bulk of silicon where they are injected into the external circuit producing a current signal. Besides the depletion region field, a strong inversion layer amplifies the separation process meanwhile hinders the excess charge recombination at the interface [23–25]. The electrical conductivity of organic PEDOT:PSS semiconductor can be manipulated by treatment with the polar organic solvents like dimethyl sulfoxide (DMSO) [25–27] and perfluorooctane sulfonic acid (PFOSA) [28] which may substantially affect the photodetection metrics of PEDOT:PSS/Si heterojunction. Herein, we study the optical responsivity of the PEDOT:PSS/Si heterojunction in a broad range of spectrum from UV to IR and monitor both the photocurrent and photovoltage response over a broad range of optical powers from nano to milli-watt intensities in order to gain reliable information on the dynamical range, signal-to-noise ratio, and noise equivalent power. The effect of organic layer conductivity on the performance of the photodetector is also investigated.

2. Experimental details

Lightly n-doped silicon wafer with 300 nm oxide layer was used to fabricate the hybrid devices. At first, the buffer layer was removed on the selected regions by wet chemical etching. In order to prevent surface oxidation, the samples were kept in Nitrogen atmosphere prior to the deposition of organic layer. The hybrid photodetectors were prepared by spin-coating the aqueous PEDOT:PSS solution (CLEVIOS PH1000, resistivity < 0.0012 Ω.cm, solid content 1.0–1.3 wt% (in water) , viscosity

* Corresponding author.
E-mail address: y.abdi@ut.ac.ir (Y. Abdi).
[1] AN and AM contributed equally to this work.

https://doi.org/10.1016/j.mseb.2021.115260
Received 22 October 2020; Received in revised form 22 April 2021; Accepted 19 May 2021
Available online 27 May 2021

< 50 mPa.s , PEDOT:PSS ratio 1:2.5) onto silicon substrates followed by heating at 110 °C under N2 gas. In order to study the effect of organic layer conductivity, we have prepared two sets of HOIPs utilizing pristine and DMSO-treated PEDOT:PSS organic layers. With inclusion of 5% dimethyl sulfoxide into the aqueous solution of pristine PEDOT:PSS, the average 4-point conductivity of PEDOT:PSS layer was improved by a factor of 3 × 10^3 from 0.25 S.cm^{-1} (pristine) to 790 S.cm^{-1} (DMSO-treated). Active area of the fabricated HOIPs ranges from A = 25 mm^2 to A = 49 mm^2. In order to ensure a stabilized performance, the experiments were performed after 20 days storage of the HOIPs in ambiance.

3. Results and discussion

Optical image and schematic representation of a hybrid photodiode with energy-band diagram of PEDOT:PSS/Si heterojunction are represented in Fig. 1(a, b). Atomic Force Microscope (AFM) topographic images of pristine and doped PEDOT:PSS with root mean square of surface roughness are shown in Fig. 1(c,d), respectively. Cross-sectional scanning electron microscopy (SEM) image of the device is also presented in Fig. 1(e). Spin coated PEDOT:PSS layer has approximately 270 nm thickness. 80–95% light absorption can be approved by the absorption spectra of the sample provided in Fig. 1(f). Fig. 1(g) shows the current–voltage characteristics in dark and under different intensities of incident light (λ = 656 nm). Reverse-bias current increases considerably with the incident optical power so that at mW intensities the rectifying character of heterojunction thoroughly disappears. Rectification ratio which is defined as $R_{rect}(V)=|I(+v)|/|I(-v)|$, decreases from $R_{rect} \cong 10^4$ in dark to $R_{rect} \cong 10^0$ at the 2 V under P≅1 mW illumination. Rectification ratio at different voltages has different values. Only when we consider ± 2 V, we get rectification value of 10^4. This corresponds to an I_{on}/I_{off} ratio exceeding 10^4 which indicates an extreme sensitivity of HOIP upon illumination. The current–voltage characteristics and the diode parameters are provided and discussed in detail in supplementary material (see S1 and the related discussion).

Photodetection figures of merit of the DMSO-treated PEDOT:PSS/Si heterojunction are presented in Fig. 2. The equivalent photodetection properties of pristine HOIP are provided in the supplementary materials S2 and S3. Fig. 2(a) presents photocurrent $I_{PC} = I_{light} - I_{dark}$ as a function of the bias voltage. At a fixed intensity of incident light, I_{PC} initially rises by decreasing the bias voltage and then exhibits a saturated plateau at the large reverse voltages. By increasing the reverse bias voltage, the width of transition region increases assisting the collection of excess photogenerated carriers. Photocurrent versus the intensity of incident light is represented in Fig. 2(b). At the bias voltages lower than $V_b \cong -2V$, I_{PC} remains linear approximately over six decades of the optical power leading to an excellent linear dynamic range of $LDR = 20\log(P_{max}/P_{min}) = 118dB$. Both photocurrent and LDR vary with bias voltage. As is shown in Fig. 2(c), for small bias voltages I_{PC} saturates at high optical powers. As reverse bias increases, the saturation region gradually disappears and the photocurrent varies linearly in the whole range of tested intensities. As a result, the linear dynamic range increases from 94 dB at zero bias to 118 dB at V_b = -2V. In this regard, bias voltage provides a decent control for tuning photocurrent at the higher optical powers. From the same data, differential photocurrent responsivity $R_I = dI_{PC}/dP$ of the DMSO-treated HOIP, determined from the slope of I_{PC} versus the intensity, is obtained as $R_I = 164 \pm 14$ mA/W which is nearly 20% higher than the pristine HOIP with $R_I = 137 \pm 9$ mA/W.

Noise level of a photodetector is an imperative character as it ultimately regulates the device performance upon low-level excitation. Fig. 2(d) shows the photocurrent spectral density (V_b = -2V) upon low intensities of the incident light. Spectral density is obtained through the fast-Fourier transformation of the photocurrent versus time data. It is seen that the Flicker 1/f-noise dominates the background fluctuations at f < 2 Hz. At the higher frequencies, the spectrum exhibits frequency-independent white character (inset of Fig. 2(d)) which is the characteristic of Johnson-Nyquist thermal noise given by $I_{th} = \sqrt{4k_BT/R}$ with R being the resistance of the device [29]. Utilizing the differential resistance of dark I-V curve at V_b = -2 V, we obtain $I_{th} = 0.016pA/\sqrt{Hz}$ for the DMSO-treated HOIP which is almost two orders of magnitude lower than the device noise floor. By analyzing the dark current spectral density, we conclude that the response upon low-level intensities should be limited by the leakage current (supplementary material S4). Noise equivalent power (NEP) is defined as the rms of the optical power with a signal-to-noise ratio (SNR) of one in a 1-Hz bandwidth. NEP is directly determined from the SNR of photocurrent spectral density [30]. At the

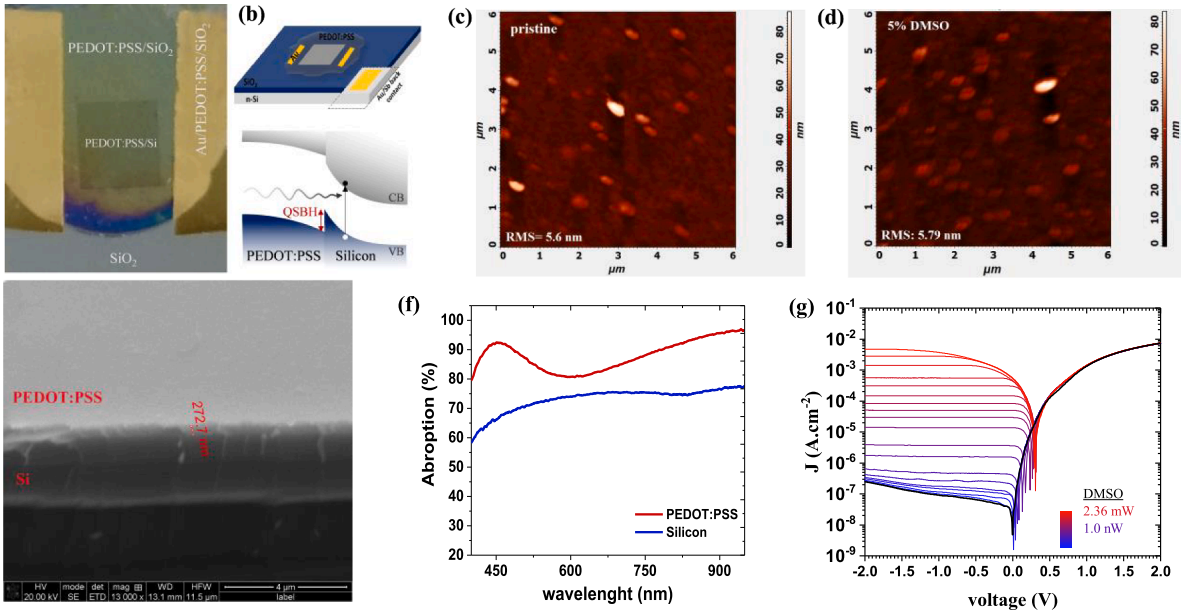

Fig. 1. (a) Optical image (top view) and (b) schematic representation of a hybrid PEDOT:PSS/Si photodiode. Area of the square window (PEDOT:PSS/Si) is 5 × 5 mm^2 with Energy band diagram at PEDOT:PSS/Si heterojunction. QSBH demonstrates the quasi-Schottky barrier at the hybrid interface. (c, d) AFM images of pristine and 5% DMSO-treated PEDOT:PSS. Root mean square of surface roughness are shown. (e) The cross-sectional SEM image of the device. (f) Absorption spectra of Si and PEDOT:PSS/Si. (g) Current-voltage in darkness (black) and under different intensities of 656 nm illumination.

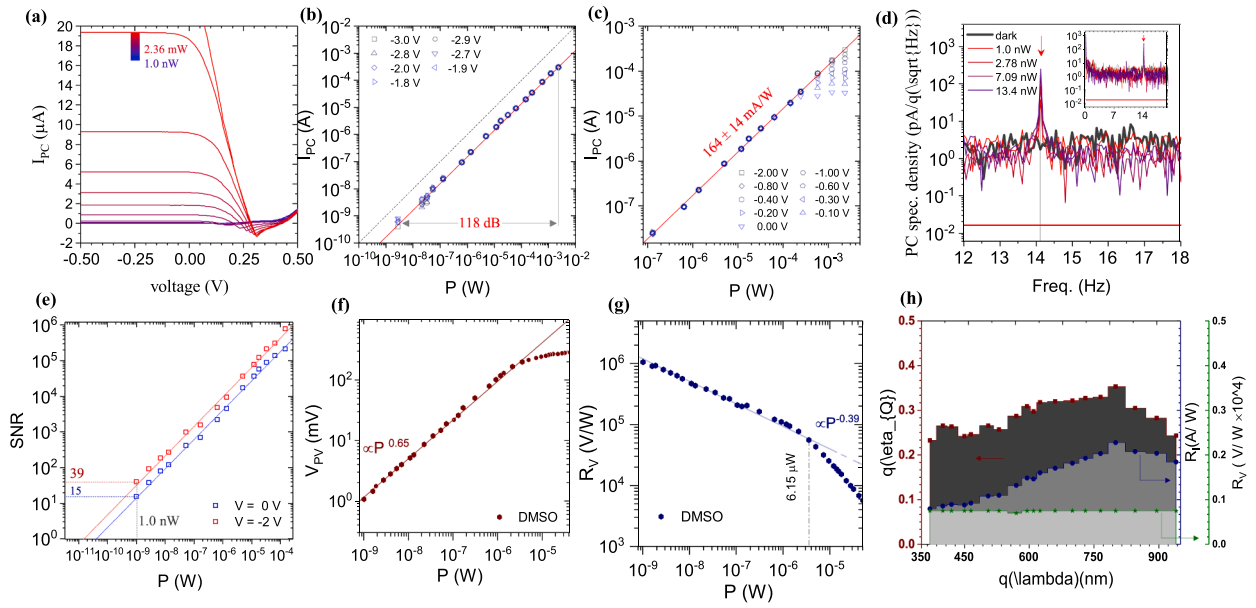

Fig. 2. Performance characteristics of DMSO-treated PEDOT:PSS/Si heterojunction. (a) Photocurrent versus bias voltage. (b) Photocurrent versus optical power. Red line shows linear fit to the experimental data. (c) The dependence of photocurrent on bias voltage at high incident powers. (d) Photocurrent spectral density at low level intensities and V_b = -2 V. The intensity of incident light is modulated at 14 Hz. Red line shows Johnson-Nyquist thermal noise. Inset represents spectral density in the frequency range of 0.1–20 Hz. (e) Signal-to-noise ratio at V_b = 0 and V_b = -2 V extracted from the photocurrent spectral density. Lines represent linear extrapolation to SNR = 1. (f) Photovoltage versus intensity of incident light. Dashed lines represent power-law fittings to the experimental data. (g) Responsivity as a function of illumination power. (h) Spectral quantum efficiency and the photocurrent and photovoltage responsivity of DMSO-treated HOIP. (For interpretation of the references to colour in this figure legend, the reader is referred to the web version of this article.)

incident intensity of 1.0 nW, the SNR of DMSO-treated HOIP is obtained as 15 and 39 at V_b = 0 and V_b = -2V, respectively (Fig. 2(e)). Linear extrapolation of the experimental data to SNR = 1 conducts a noise equivalent power of 40 $pA/\sqrt{Hz}$ at zero bias which decreases to 16 $pA/\sqrt{Hz}$ at V_b = -2 V. Such a low NEP indicates the suitability of PEDOT:PSS/Si HOIPs for the low-intensity light detection. Specific detectivity $\left(D^* = \sqrt{A/NEP}\right)$ of the DMSO-treated sample at V_b = -2 V is determined as $D^* = 1.5 \times 10^{10}$ Jones (Jones $= \mathrm{cm}.\sqrt{Hz}/W$). In comparison, the noise equivalent power and the detectivity of the pristine HOIP at V_b = -2 V are obtained as NEP = 83 $pW/\sqrt{Hz}$ and $D^* = 2 \times 10^9$ Jones (supplementary material S3). Under open-circuit conditions, the photovoltage response of the devise versus the optical power and the corresponding photovoltage responsivity are presented in Fig. 2(f) and Fig. 2(g), respectively. As shown from these figures, the responsivity of DMSO-treated PEDOT:PSS/Si exceeds 2×10^6 V/W at the lower intensities. It should be noted that R_V exhibits two distinct power-law dependences on the incident light intensity, which are fairly separated at 6.15 μW.

High-gain broadband photodetectors have achieved great progress with response range covering UV–VIS-NIR region. For instance, photomultiplicaiton optical photodetectors exhibit great potential in real application with EQE exceeding 100% under low bias [31–33]. In order to test the broad band sensitivity of the device, the spectral quantum efficiency and responsivity are represented in Fig. 2(h). R_I increases from 90 mA/W at 400 nm to its maximum value of 230 mA/W at 800 nm and subsequently declines to 185 mA/W at 940 nm. The high responsivity of 90–230 mA/W which is achieved for our photodetector, is one order of magnitude higher than the previously reported PEDOT:PSS-based detectors [19,21]. This measurement is carried out under the 3×10^{-4} W illuminations. Consequently, based on the results of Fig. 2 (g), R_v for this optical intensities is obtained in the range of 10^3 V/W. As shown in Fig. 2(h), R_v is almost constant for all the wavelengths in the range.

The Internal Quantum Efficiency (IQE) is defined as the ratio of the number of electron-hole (e-h) pairs or charge carriers generated to the number of absorbed incident photons within the active layer of the device. The internal spectral quantum efficiency along with the corresponding data of responsivity is also represented in Fig. 2(h).

Fig. 3 presents the response dynamics of HOIPs. Photocurrent in Fig. 3(a) and Fig. 3(b) is normalized to its maximum value. Under a fixed intensity of incident light, both response and recovery speed of hybrid photodetectors improve with the bias voltage which can be understood based on the electric field enhancement at transition region. The DMSO-treated PEDOT:PSS/Si exhibits a faster dynamics. At V_b = -2 V, the characteristic rise and decay time of the DMSO-treated HOIP are obtained as τ_{rise} = 28 μs and τ_{dec} = 40 μs. In comparison, the pristine HOIP displays τ_{rise} = 129 μs and τ_{dec} = 146 μs at the same bias voltage (Fig. 3 (c)). Accordingly, the improved conductivity of DMSO-treated PEDOT:PSS conducts a 4-fold enhancement in the photoresponse dynamics [22]. It is worth to note that diffusion of excess electrons in the neutral region of silicon is the ultimate limiting factor in the speed of fabricated photodiodes. A large fraction of incident photons is absorbed in the bulk of silicon far from the depletion region at interface [34]. The photogenerated holes should diffuse into the transition region where they are delivered to the organic layer by drift current. On the other hand, the excess electrons have to diffusive through the entire thickness of Si to get the back contact leading to a considerable delay in device response. The time required for electrons to diffuse toward the back contact can be estimated from $t_d = \frac{4x^2}{\pi^2 D_n}$ [22]. Here, x is the thickness of silicon (400 μm) and D_n is diffusion coefficient of electrons that can be obtained by $D_n = \left(\frac{k_B T}{e}\right)\mu_e$ with μ_e = 1500 $\mathrm{cm^2 V^{-1} s^{-1}}$ being electron mobility. Accordingly, diffusion of excess electrons toward the back contact requires $t_D \cong 17\mu s$ very close to the rise and decay time at V_b = -2 V. The neutral region of silicon also contributes in the photodetector noise through the series resistance. The speed of HOIPs can be further improved by either reducing the thickness of neutral region or employing an additional doping (i.e. n +) to the back side of silicon.

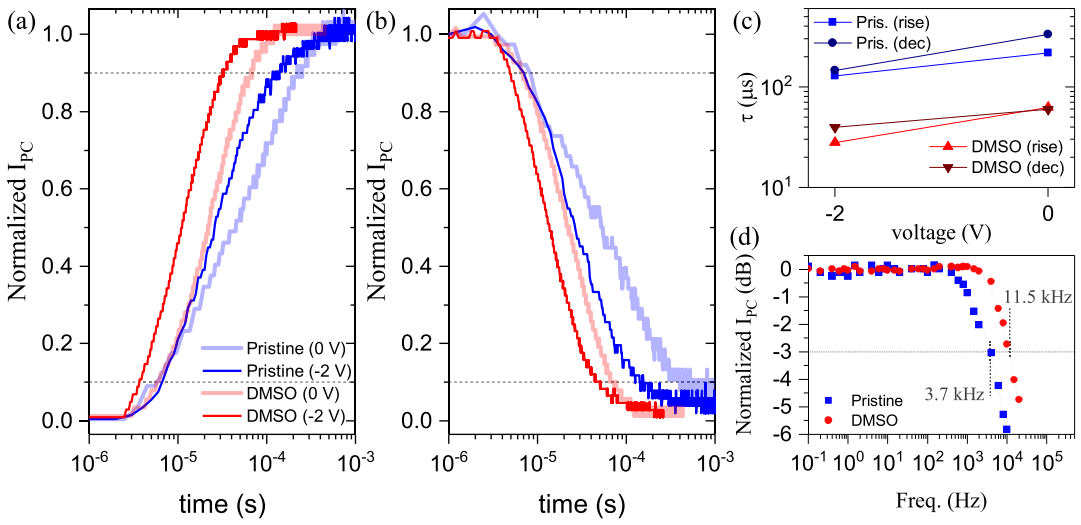

Fig. 3. Real-time (a) response and (b) recovery of the normalized photocurrent (I_{PC}/I_{PC}^{max}). (c) Characteristic 10% − 90% rise time and 90% − 10% decay time of HOIPs as function of bias. (d) Normalized photocurrent versus modulation frequency of incident light ($V_b = -2$).

Normalized photocurrent $10\log[I_{PC}(f)/I_{PC}(0.1Hz)]$ versus the modulation frequency of incident light is shown in Fig. 3(d). At V_b = -2 V, the −3dB response bandwidth of pristine and DMSO-treated HOIPs are obtained as B = 3.7 kHz and B = 11.5 kHz, respectively. The cut-off frequency of 11 kHz corresponds to a frame rate of 11,000 frame-per-seconds (FPS) which is quite appealing for high-speed photography, spectrophotometry, remote control sensors, digital imaging, and monitoring chemical reactions that typically require a millisecond-order response time. Response uniformity upon long-term exposure to cyclic illumination and performance deterioration of DMSO-treated PEDOT:PSS/Si photodiode through storage in ambiance are provided in the supplementary material S5.

A comparative summary of our main findings and previous studies is provided in Table 1. It is worth to point out some remarks. First, our results show that the fabricated simple planar PEDOT:PSS/Si heterojunction could conduct excellent sensitivity with out-standing figures of merit such as large LDR and fast response in PC operational mode and ultra-high responsivity in PV mode. Second, indirect estimation of detectivity (from responsivity and dark current) provides only a rough, often inflated, assessment. As a delicate quantity, specific detectivity requires to be resolved by a direct approach. In the case of planar PEDOT:PSS/Si (with 400 μm-thick Si), our meticulous assessments suggest that the specific detectivity is at best around 10^{10} Jones. Nonetheless the hybrid photodetectors display remarkable records in terms of sensitivity upon Nano-watt illumination, LDR, speed (PC mode), and responsivity. This clarifies long-period reliability of hybrid organic–inorganic photodetectors.

4. Conclusion

In conclusion, we demonstrate the broad band photodetection of DMSO-treated PEDOT:PSS/Si in the range of 400–950 nm. Also, the vital role of organic layer conductivity in the speed and low-level light detection properties of the device is demonstrated. In both the photocurrent and photovoltage operational modes, DMSO-treated PEDOT:PSS/Si heterojunction displays a large LDR and high responsivity. These results show that the HOIPs are quite appealing for a vast variety of optoelectronic applications. In addition, considering low NEP of 16 pW/$\sqrt{Hz}$, these photodiodes are also very suitable for the detection of extreme low powers. The straightforward and low-temperature process of organic layer deposition presents an economic alternative for the high-temperature diffusion process used in the conventional silicon photodiodes. Our study on the planar PE-DOT:PSS/Si provides the preliminary stage for more advanced hybrid organic–inorganic heterojunction photodiodes including avalanche, and point-contact detectors.

Table 1
Photoresponse characteristics of PEDOT:PSS/Si HOIPs.

Photocurrent (PC)							Photovoltage (PV)					
Structure & test wavelength	R_I (mA/W)	D* (Jones)	LDR (dB)	B (kHz)	τ_{rise} (μs)	τ_{dec} (μs)	R_V (V/W)	D* (Jones)	B (kHz)	τ_{rise} (μs)	τ_{dec} (μs)	Ref.
PEDOT:PSS/Si nanowire (λ = 650 nm)[a]	20	4×10^{11}[b]	42	–	–	–	–	–	40.6	3.2	55.4	[19]
GQD-PEDOT:PSS/Si (λ = 532 nm) [a]	1000[c]	8×10^{11}[b]	–	–	80	70	–	–	–	–	–	[20]
PEDOT:PSS/Ga_2O_3/Si (λ = 255 nm)[a]	12	–	–	–	60×10^3	88×10^3	–	–	–	–	–	[21]
PEDOT:PSS/Si (λ = 656 nm)[d]	137	2×10^9	85	3.7	129	146	7×10^5	8.7×10^9	0.037	280	330×10^3	This work
DMSO-PEDOT:PSS/Si (λ = 656 nm)[d]	164	1.5×10^{10}	118	11.5	28	40	2×10^6	1.8×10^{10}	0.450	47	11×10^3	This work

[a] Measured at V_b = 0 V.
[b] Estimated indirectly from responsivity and dark current.
[c] Measured at P = 2.52 μW.
[d] PC data are acquired at V_b = -2 V.

Declaration of Competing Interest

The authors declare that they have no known competing financial interests or personal relationships that could have appeared to influence the work reported in this paper.

Acknowledgment

The authors acknowledge Iran National Science Foundation (INSF) , Institute of quantum science and technology of University of Tehran and Iran Science Elites Federation (ISEF) for partial financial support.

Appendix A. Supplementary data

Supplementary data to this article can be found online at https://doi.org/10.1016/j.mseb.2021.115260.

References

[1] P. Singh, S.K. Srivastava, B. Sivaiah, P. Prathap, C.M.S. Rauthan, Enhanced photovoltaic performance of PEDOT: PSS/Si solar cells using hierarchical light trapping scheme, Sol. Energy 170 (2018) 221.
[2] Y. Xia, S. Dai, Review on applications of PEDOTs and PEDOT:PSS in perovskite solar cells, J. Mater. Sci.: Mater. Electron. 1 (2020).
[3] Z.P. Ling, Z. Xin, G. Kaur, C. Ke, R. Stangl, Ultra-thin ALD-AlOx/PEDOT: PSS hole selective passivated contacts: An attractive low cost approach to increase solar cell performance, Sol. Energy Mater. Sol. Cells 185 (2018) 477.
[4] S. Jeong, E.C. Garnett, S. Wang, Z. Yu, S. Fan, M.L. Brongersma, M.D. McGehee, Y. i. Cui, Hybrid silicon nanocone-polymer solar cells, Nano Lett. 12 (6) (2012) 2971–2976.
[5] W. Li, N. Cheng, Y. Cao, Z. Zhao, Z. Xiao, W. Zi, Z. Sun, Boost the performance of inverted perovskite solar cells with PEDOT:PSS/graphene quantum dots composite hole transporting layer, Org. Electron. 78 (2020), 105575.
[6] P. Li, M.I.O. Mohamed, C. Xu, X. Wang, X. Tang, Electrical property modified hole transport layer (PEDOT: PSS) enhance the effciency of perovskite solar cells: Hybrid co-solvent post-treatment, Org. Electron. 78 (2020), 105582.
[7] Q. Zhang, Y. Lu, Z. Liu, H. Yu, Y. Duan, L. Liu, S. Chen, W. Huang, Highly effcient organic-inorganic hybrid perovskite quantum dot/nanocrystal light-emitting diodes using graphene electrode and modified PEDOT:PSS, Org. Electron. 72 (2019) 30.
[8] X. Jiang, Y. Ma, Y. Tian, A. Wang, A. Wang, S. Zhang, S. Wang, Z. Du, High-efficiency and stable quantum dot light-emitting diodes with staircase v2o5/PEDOT:PSS hole injection layer interface barrier, Org. Electron. 78 (2020), 105589.
[9] J. Fan, S.S. Rezaie, M. Facchini-Rakovich, D. Gudi, C. Montemagno, M. Gupta, Tuning PEDOT:PSS conductivity to obtain complementary organic electrochemical transistor, Org. Electron. 66 (2019) 148.
[10] T. Lee, W. Kwon, M. Park, Highly conductive, transparent and metal-free electrodes with a PEDOT:PSS/SWNT bilayer for high-performance organic thin film transistors, Org. Electron. 67 (2019) 26.
[11] M. Javadi, M. Gholami, H. Torbatiyan, Y. Abdi, Hybrid organic/inorganic position-sensitive detectors based on PEDOT:PSS/n-Si, Appl. Phys. Lett. 112 (2018), 113302.
[12] M. Zhu, K. Meng, C. Xu, J. Zhang, G. Ni, Lateral photovoltaic effect in ITO/PEDOT: PSS/MEHPPV:PCBM/al organic photovoltaic cells, Org. Electron. 78 (2020), 105585.
[13] H.-D. Um, D. Choi, A. Choi, J.H. Seo, K. Seo, Embedded metal electrode for organic-inorganic hybrid nanowire solar cells, ACS Nano 11 (6) (2017) 6218–6224.
[14] J. He, P. Gao, Z. Yang, J. Yu, W. Yu, Y.u. Zhang, J. Sheng, J. Ye, J.C. Amine, Y. i. Cui, Silicon/organic hybrid solar cells with 16.2% efficiency and improved stability by formation of conformal heterojunction coating and moisture-resistant capping layer, Adv. Mater. 29 (15) (2017) 1606321, https://doi.org/10.1002/adma.201606321.
[15] L. Zhang, Z. Wang, H. Lin, W. Wang, J. Wang, H. Zhang, J. Sheng, S. Wu, P. Gao, J. Ye, T. Yu, Thickness modulated passivation properties of PEDOT:PSS layers over crystalline silicon wafers in back junction organic/silicon solar cells, Nanotechnology 30 (2019), 195401.
[16] M.-U. Halbich, D. Zielke, R. Gogolin, R. Sauer-Stieglitz, W. Lovenich, J. Schmidt, Improved surface passivation and reduced parasitic absorption in PEDOT:PSS/c-Si heterojunction solar cells through the admixture of sorbitol, Sci. Rep. 9 (2019) 9775.
[17] A.S. Islam, M.E. Karim, A. Rajib, Y. Nasuno, T. Ukai, S. Kurosu, M. Tokuda, Y. Fujii, Y. Nakajima, T. Hanajiri, H. Shirai, Chemical mist deposition of organic for effcient front- and back-PEDOT:PSS/crystalline Si heterojunction solar cells, Appl. Phys. Lett. 114 (2019), 193901.
[18] J.P. Thomas, Q. Shi, M. Abd-Ellah, L. Zhang, N.F. Heinig, K.T. Leung, Charge transfer in nanowire -embedded PEDOT:PSS and planar heterojunction solar cells, ACS Appl. Mater. Interfaces 12 (2020) 11459.
[19] Z. Liang, P. Zeng, P. Liu, C. Zhao, W. Xie, W. Mai, Interface engineering to boost photoresponse performance of self-powered, broad-bandwidth PEDOT: PSS/Si heterojunction photodetector, ACS Appl. Mater. Interfaces 8 (2016) 19158.
[20] M.-L. Tsai, D.-S. Tsai, L. Tang, L.-J. Chen, S.P. Lau, J.-H. He, Omnidirectional harvesting of weak light using a graphene quantum dot-modified organic/silicon hybrid device, ACS Nano 11 (5) (2017) 4564–4570.
[21] D. Zhang, W. Zheng, R. Lin, Y. Li, F. Huang, Ultrahigh EQE (15%) solar-blind UV photovoltaic detector with organic{inorganic heterojunction via dual built-in fields enhanced photogenerated carrier separation efficiency mechanism, Adv. Funct. Mater. 29 (26) (2019) 1900935, https://doi.org/10.1002/adfm.v29.2610.1002/adfm.201900935.
[22] A. Mosaddegh, A. Noroozi, M. Javadi, Y. Abdi, Ultrahigh photovoltage responsivity of PEDOT:PSS-silicon hybrid heterojunction photodiodes, Appl. Phys. Lett. 117 (2020), 073301.
[23] A.S. Erickson, A. Zohar, D. Cahen, n-Si-organic inversion layer interfaces: A low temperature deposition method for forming a p-n homojunction in n-Si, Adv. Energy Mater. 4 (2014) 1301724.
[24] J. Zhu, X. Yang, J. Sheng, P. Gao, J. Ye, Double layered PEDOT:PSS films inducing strong inversion layers in organic/silicon hybrid heterojunction solar cells, ACS Applied Energy Materials 1 (2018) 2874.
[25] R. Wang, Y. Wang, C. Wu, T. Zhai, J. Yang, B. Sun, S. Duhm, N. Koch, Direct observation of conductive polymer induced inversion layer in n-Si and correlation to solar cell performance, Adv. Funct. Mater. 30 (4) (2020) 1903440, https://doi.org/10.1002/adfm.v30.410.1002/adfm.201903440.
[26] H. Shi, C. Liu, Q. Jiang, J. Xu, Effective approaches to improve the electrical conductivity of PEDOT:PSS: A review, Adv. Electron. Mater. 1 (2015) 1500017.
[27] Q. Wei, M. Mukaida, Y. Naitoh, T. Ishida, Morphological change and mobility enhancement in PEDOT:PSS by adding co-solvents, Adv. Mater. 25 (2013) 2831.
[28] T. Kim, S. Park, J. Seo, C.W. Lee, J.-M. Kim, Highly conductive PEDOT:PSS with enhanced chemical stability, Org. Electron. 74 (2019) 77.
[29] C. Fuentes-Hernandez, W.-F. Chou, T.M. Khan, L. Diniz, J. Lukens, F.A. Larrain, V. A. Rodriguez-Toro, B. Kippelen, Large-area low-noise flexible organic photodiodes for detecting faint visible light, Science 370 (6517) (2020) 698–701.
[30] Antonio. Di Bartolomeo,, Graphene Schottky diodes: An experimental review of the rectifying graphene/semiconductor heterojunction, Phys. Rep. 606 (2016) 1.
[31] Z. Zhao, C. Xu, L. Niu, X. Zhang, F. Zhang, Recent progress on broadband organic photodetectors and their applications, Laser Photonics Rev. 14 (11) (2020) 2000262, https://doi.org/10.1002/lpor.v14.1110.1002/lpor.202000262.
[32] Z. Zhao, J. Wang, C. Xu, K. Yang, F. Zhao, K. Wang, X. Zhang, F. Zhang, Photomultiplication type broad response organic photodetectors with one absorber layer and one multiplication layer, J. Phys. Chem. Lett. 11 (2) (2020) 366–373.
[33] Z. Zhao, C. Li, L. Shen, X. Zhang, F. Zhang, Photomultiplication type organic photodetectors based on electron tunneling injection, Nanoscale 12 (2) (2020) 1091–1099.
[34] S.M. Sze, L. Yiming, K. Ng, Kwok, Physics of semiconductor devices, John Wiley & Sons, 2021.